Second Sound in He II

Otis Chodosh, Jeremy Hiatt, Samir Shah, and Ning Yan
Department of Physics, Stanford University
All authors contributing equally
(Dated: March 21, 2008)

The speed of second sound in ^{4}He is measured from ~ 1.3 K to ~ 2.1 K using both resonance and time of flight methods in a closed cavity driven by and monitored with a pair of Nuclepore filter paper transducers. The resonance method yielded a very close fit to Wang (1987), and the time of flight method also yielded fairly comparable data.

I. INTRODUCTION

In this paper we examine the phenomenon known as *second sound* in superfluid ^{4}He. Second sound is a wave that, in contrast to first sound (ordinary sound), is not a pressure wave; instead is an entropy wave.

II. THEORY

One theoretical model for superfluid ^{4}He (also known as He II) involves considering the fluid as being composed of both superfluid and normal particles. This is certainly not how He II actually works; in fact, because ^{4}He is a boson, all of the particles are identical, and as such cannot actually be separated into the two categories. However, this model describes many of the observed He II phenomena quite well, including second sound.

Assigning a relative density to each type of particle, ρ_s and ρ_n, we have that the total density is

$$\rho = \rho_s + \rho_n \tag{1}$$

and denoting the superfluid and normal velocities, as $\mathbf{v_s}$ and $\mathbf{v_n}$ we define $\mathbf{j}$, the mass flux of superfluid to be

$$\mathbf{j} = \rho_s \mathbf{v_s} + \rho_n \mathbf{v_n} \tag{2}$$

Neglecting gravity and letting S denote entropy, P denote pressure and T denote temperature, the hydrodynamic equations[1] are

$$\frac{\partial \rho}{\partial t} + \rho_s \nabla \cdot \mathbf{v_s} + \rho_n \nabla \cdot \mathbf{v_n} = 0 \text{ (mass conservation)} \tag{3}$$

$$\frac{\partial \mathbf{v_s}}{\partial t} + \frac{1}{\rho}\nabla P - S\nabla T = 0 \text{ (momentum conservation)} \tag{4}$$

$$\frac{\partial \mathbf{v_n}}{\partial t} + \frac{1}{\rho}\nabla P + \frac{\rho_s}{\rho_n} S\nabla T = 0 \text{ (momentum conservation)} \tag{5}$$

$$\frac{\partial}{\partial t}(\rho S) + \nabla \cdot (\rho S \mathbf{v_n}) = 0 \text{ (entropy conservation)} \tag{6}$$

These equations admit two different wave equations[2]. First sound, a pressure wave is given by

$$\frac{\partial^2 \rho}{\partial t^2} = u_1^2 \nabla^2 \rho \tag{7}$$

where the first sound velocity is given by

$$u_1 = \left(\frac{\partial P}{\partial \rho}\right)_S^{1/2} \tag{8}$$

Second sound, an entropy wave is given by

$$\frac{\partial^2 S}{\partial t^2} = u_2^2 \nabla^2 S \tag{9}$$

where the second sound velocity is given by

$$u_2 = \left(\frac{\rho_s}{\rho_n}\frac{TS^2}{C_p}\right)^{1/2} \tag{10}$$

where C_p is the specific heat.

It can be shown that in first sound $\mathbf{v_s} = \mathbf{v_n}$, so it corresponds to a traditional wave in a fluid because the whole fluid is moving as one unit. Conversely, in second sound, $j = \rho_s \mathbf{v_s} + \rho_n \mathbf{v_n} = 0$, and the total density, ρ is constant. Thus the relative densities oscillate, as opposed to the total density.

Traditionally, second sound is generated by an oscillating heat source and detected by a thermometer. However, it is also possible (as has been done in this paper) to generate and detect second sound using an oscillating porous membrane. That this method also generates second sound is a striking example of the two fluid model's

[1] The given hydrodynamic equations are approximations that neglect irreversible effects such as dissipation, as well as other higher order effects.

[2] Adriaans, M.J. *High Resolution Measurements of the Second Sound Velocity Near the Lambda Transition in Superfluid Helium-4*, Thesis, Dept. Physics, Stanford University (1994)

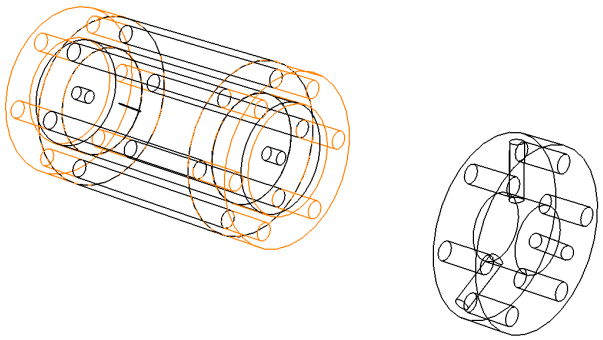

FIG. 1: A wireframe view of the closed geometry. Six threaded rods and nuts were used to connect the mounting bracket (right) to the resonating assembly (left). The brown color marks the transducer assemblies.

effectiveness in explaining phenomena present in He II. In the model, the superfluid will have a low enough viscosity that it can pass through the pores, while no significant amount of normal fluid will be able to pass through the pores because it has a much higher viscosity. As a result, the relative densities will oscillate, creating exactly the same effect that is seen in the original second sound experiment with a oscillating heat source and thermometer.

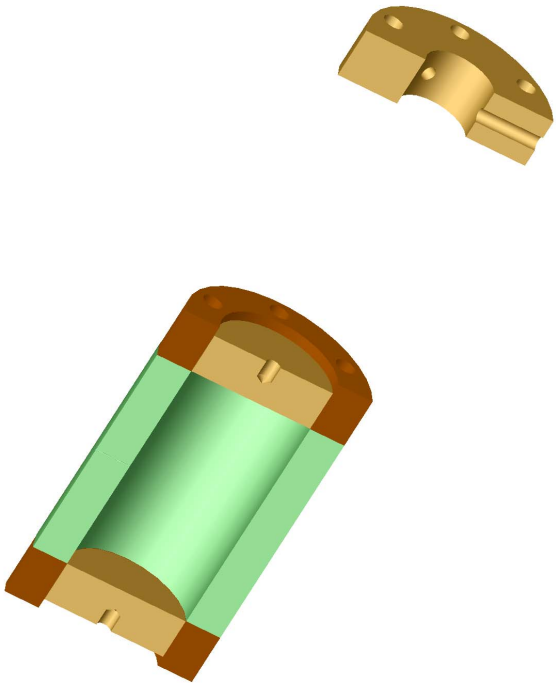

FIG. 2: A cross section view of the closed geometry. The green section is the resonating chamber, and the red sections are the outer transducers.

III. EXPERIMENTAL DESIGN

Second sound velocity was ascertained in two ways: by measuring resonance frequencies of the transducer chamber, and by measuring the time of flight of second-sound pulses over the known chamber length. Appropriately low temperatures were realized by immersing the apparatus Dewar in a surrounding Dewar of liquid nitrogen and lowering the pressure with an external air pump.

A. Apparatus

The experimental apparatus is shown in Figures 1 and 2. The glass helium Dewar has a length of 36 inches and an inner diameter of 2 inches. It is sealed from the top with an o-ring gasket, which has tubes for air evacuation, helium gas insertion and electrical connectors. The apparatus is supported within the Dewar by a thin metal rod running down the center, to which it is attached with a brass flange.

The apparatus consists of two Whatman Nuclepore filters of hole size 2.0 μ on each end of a hollow cylindrical chamber of length 1.630 $\pm$ .005 inches, and inner diameter of 0.875 $\pm$ .005 inches, sandwiched in place by a transducer unit on each end of the chamber. Each Nucleopore was evaporated with gold on its chamber-facing side. The chamber has a #70 hole drilled midway between its end to facilitate helium passage. Each transducer unit consists of a ring and inner cylinder. The inner cylinder is recessed with respect to the ring by a height difference of approximately 2 mil, creating a volume between it and the Nucleopore filter. A 5 mil spacing is given between the inner diameter of the ring and the outer diameter of the inner cylinder.

Insulation and bonding between the ring and inner cylinder are achieved by wrapping the inner cylinder in 3M, #5413 Polymide Film Tape with a 2.7 mil height, and filling the radial space with Miller-Stephenson #907 epoxy. The transducers and chamber are constructed of brass. The capacitance of each transducer was measured as part of a RC circuit. The top and bottom transducers have experimental capacitances of 101 pF and 106 pF, respectively. They were constructed with gold-coated Nucleopore filters stretched across the cylindrical chamber. The gold was deposited in an electron beam evaporator with a film thickness of roughly 50nm.

Both transducers, the resonating chamber, and flange are drilled for passage of six brass threaded rods, to which nuts are added to secure the entire apparatus. The Nucleopores have holes poked in them to allow the threaded rods to pass through the entire assembly. Pressure within the helium Dewar is measured with a Pennwalt pressure gauge, connected to the air tube that passes through the top of the Dewar. The resonating chamber length was measured with a micrometer at 293K

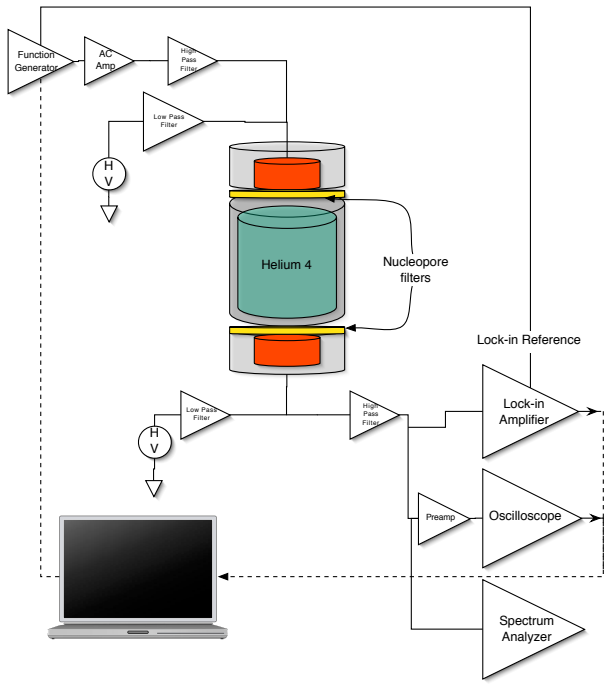

FIG. 3: Diagram of electronics and experimental setup for a frequency sweep using the "lock-in" amplifier.

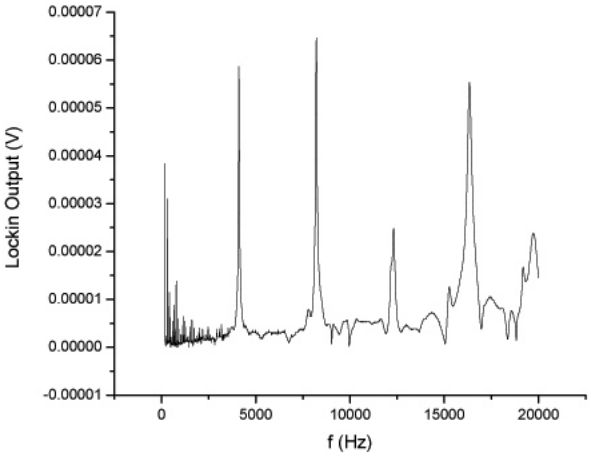

FIG. 4: A full sweep of 0 - 20 kHz in air. The resonance peaks are clearly visible.

and 77K. Our values were $L_{(293K)} = 1.6309 \pm .0002$ inches and $L_{(77K)} = 1.6261 \pm .0001$ inches, which agree with the thermal coefficient of expansion at 77K for brass of $\alpha_{(80K)} = 35.0$ [3]. For our chamber length at 4K we used $\alpha_{(0K)} \simeq 38.4$, giving $L_{(4K)} = 1.6246 \pm .0002$ inches.

[3] α_T is measured in units of $10^4 \cdot \frac{L_{(293K)} - L_{(T)}}{L_{(293K)}}$

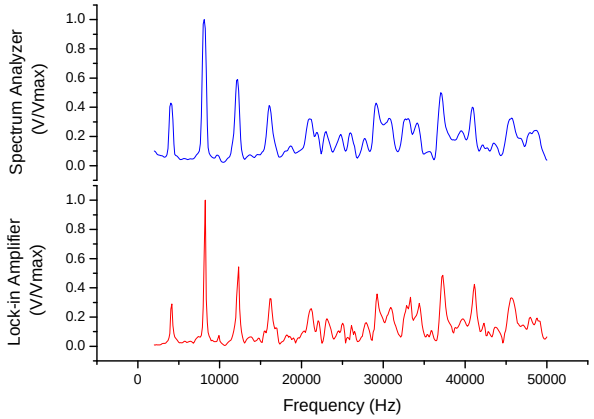

FIG. 5: A comparison in air, of a sweep using the spectrum analyzer (blue, on top) versus the "lock-in" amplifier (red, on bottom). Notice that there is a high degree of correlation between the two methods.

B. Experimental Procedure

1. *Mechanical*

The helium Dewar was first evacuated of air. The surrounding Dewar was then nearly filled with liquid nitrogen. Liquid helium was subsequently inserted within the helium Dewar through the transfer tube. The temperature within the helium Dewar was adjusted by means of a needle valve and ball valve connected in parallel to the input of the air pump.

2. *Electronics*

We attempted to measure the speed of second sound in three ways. One approach was to sweep the frequency of the drive signal and use a SR830 "lock-in" amplifier (LIA) to measure the response. Since the frequencies of the resonant modes depend on the speed of second sound, a measurement of the harmonics of the first longitudinal mode should give an accurate value for the speed of second sound. A diagram of the electronic and mechanical setup in this configuration is given in Figure 3. A sample sweep at room temperature in air is shown in Figure 4. Instead of using the "lock-in" amplifier, there was some discussion of using a Agilent DS06104A spectrum analyzer to track the output frequencies. This was discarded because the "lock-in" method had a much higher accuracy, though both methods agree to a high degree. This correlation, a verification of the experimental design, is shown in Figure 5.

An alternate approach was to drive one transducer with a pulse and measure the time until the transducer on the listening end registered the pulse. We used an Agilent 89410A oscilloscope in averaging mode and set it

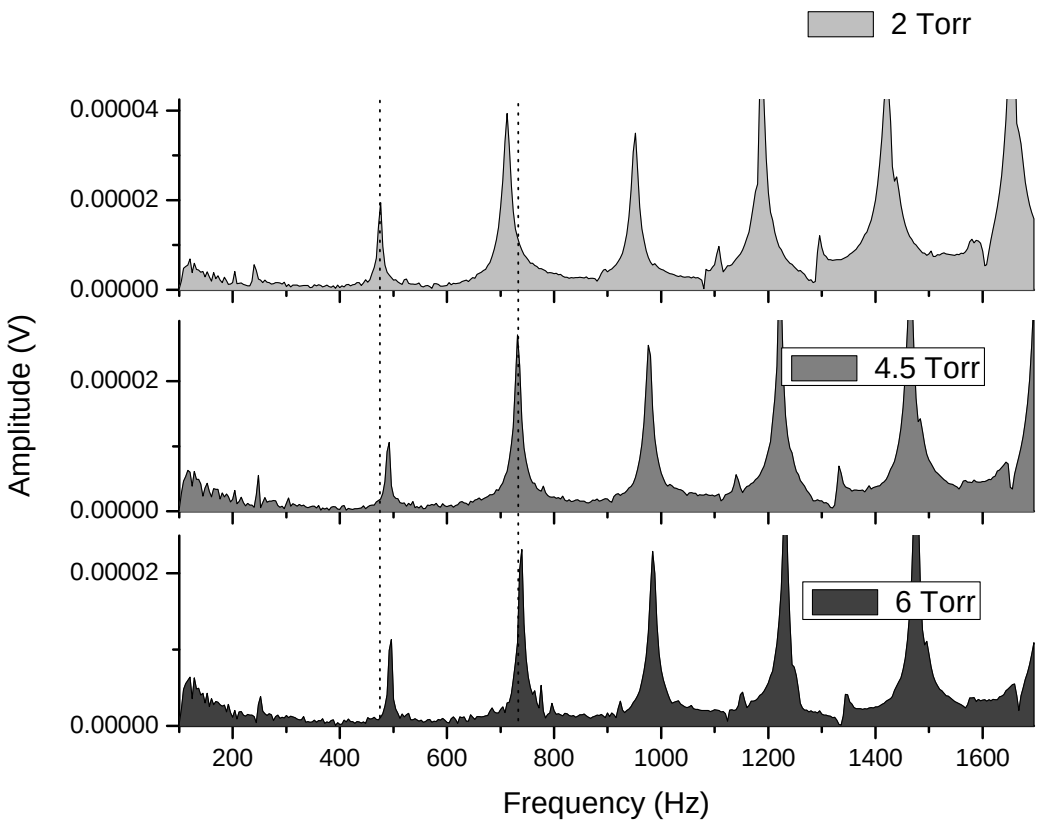

FIG. 6: A comparison of the "lock-in" sweep at various pressures (temperatures). Notice that in this range, the frequency of the harmonics increases with pressure (temperature), which corresponds to an increase in the velocity of second sound.

to trigger on the initial pulse. The time-of-flight (TOF), the time delay between the pulse and the response, can be used to calculate the speed given the distance between the two transducers.

Finally, we drove one transducer with white noise and, on the listening end, attempted to resolve the resonant frequencies with a spectrum analyzer.

The inner caps on the chamber were electrically isolated from the rest of the assembly. On the driving and listening ends, we applied an adjustable DC bias ranging from 80 V to 120 V. On the driving end, an AC signal output by an HP33120A Function Generator floated on the DC bias to induce motion in the filter. For the time-of-flight and noise measurements, it was necessary to amplify this signal; when using the "lock-in" to find resonant modes, we needed no amplification of the drive signal. For a typical measurement using the "lock-in", the input signal was a 20 V_{p-p} sine wave swept from ∼100 Hz up to ∼4 kHz. For TOF measurements, a square wave pulse was amplified up to 80 V.

IV. RESULTS

A. Data Analysis

1. Resonance

For each data set, a MATLAB routine calculated the center frequency for each peak. Then, it extracted a rough estimate for the frequency of the principle longitudinal mode by calculating the spacing between the first several peaks. With this frequency, it was then possible to infer the number for each longitudinal mode. Dividing each peak by its mode number and averaging these results gave a final estimate for the frequency of the principal mode. This frequency can then be related to the speed of second sound

$$u = 2Lf \tag{11}$$

where L is the length of the resonating chamber.

Figure 7 shows the results from a 0-10 kHz sweep of He II at 1.3 Torr. Where the longitudinal modes are

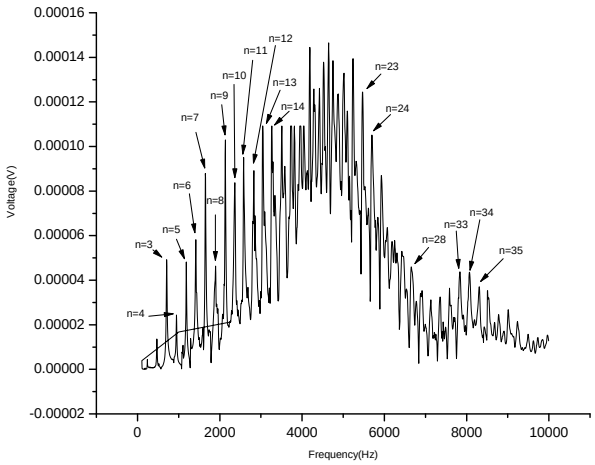

FIG. 7: Identification of longitudinal modes of a frequency sweep at $P = 1.3$ torr. n denotes the longitudinal mode number. Many of the unlabeled modes come from the effects of transverse modes, and as such are not pure longitudinal modes.

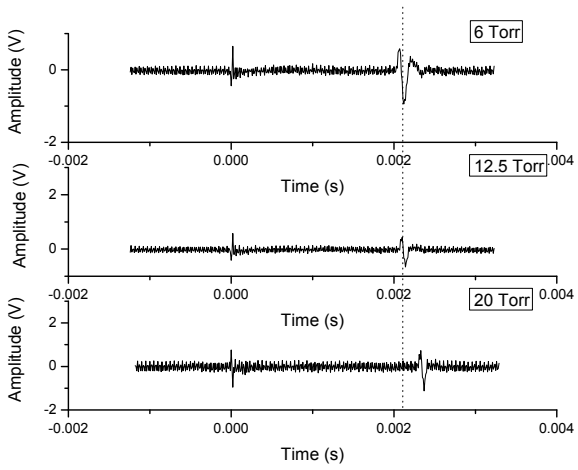

FIG. 8: TOF data varying with pressure (temperature). The TOF equivelance of Figure 6.

discernible from the transverse modes they are identified. The general form of the graph is hypothesized to be caused by the distribution of transverse modes. A statistical analysis of all the theoretically present transverse modes[4] up to and including $l = 5, m = 5$ from

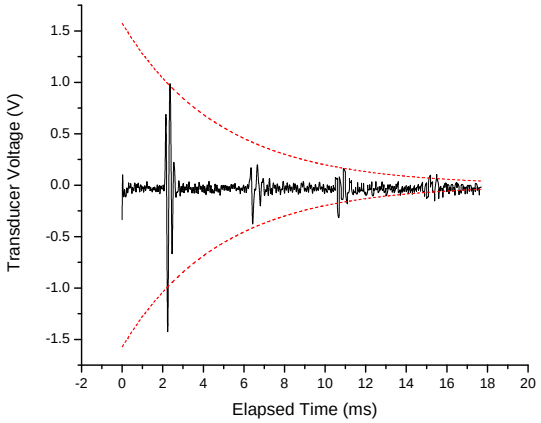

FIG. 9: TOF signal attenuation. The pulse bounces between the two transducers, decaying exponentially (in red).

0 to 10kHz yields, for this pressure range, a mean frequency of about 6267 Hz, with a standard deviation of 2288 Hz. If we account for the stronger signal of lower frequency modes, this roughly shifts the distribution to the left and explains the general form of Figure 7. The effects of the transverse modes was minimized by choosing the resonant chamber dimensions so that there was a minimal amount of degeneracies between the longitudinal resonant frequencies and the transverse modes.

2. *Time of Flight*

For each time of flight data set, a MATLAB routine extracted the time difference between the initial pulse and each response. These responses occur after odd multiples of the time interval T, which is the time for the second sound pulse to travel the length of the cavity. Averaging the extracted value of T for each ring gave a final result for the time of flight at a given temperature. The speed of second sound is simply given by

$$u = \frac{L}{t} \tag{12}$$

where L is again the cavity length.

[4] The wave number of a wave in a cylindrical cavity is given by $k_{l,m,n} = \sqrt{\left(\frac{j_{m,l}}{a}\right)^2 + \left(\frac{n\pi}{L}\right)^2}$ where L is the length, a is the radius, $l, n = 0, 1, 2, 3, \ldots$, $m = 1, 2, 3 \ldots$, and $j_{m,l}$ is the lth zero of the mth bessel function. Notice that in the limit $L >> a$, the formula reduces to $k = \frac{n\pi}{L}$. Because the formula above is derived from an inhomogenous wave equation, there will be purely longitudinal modes. These are what we use to measure u, so the other transverse modes show up as extraneous peaks in our data.

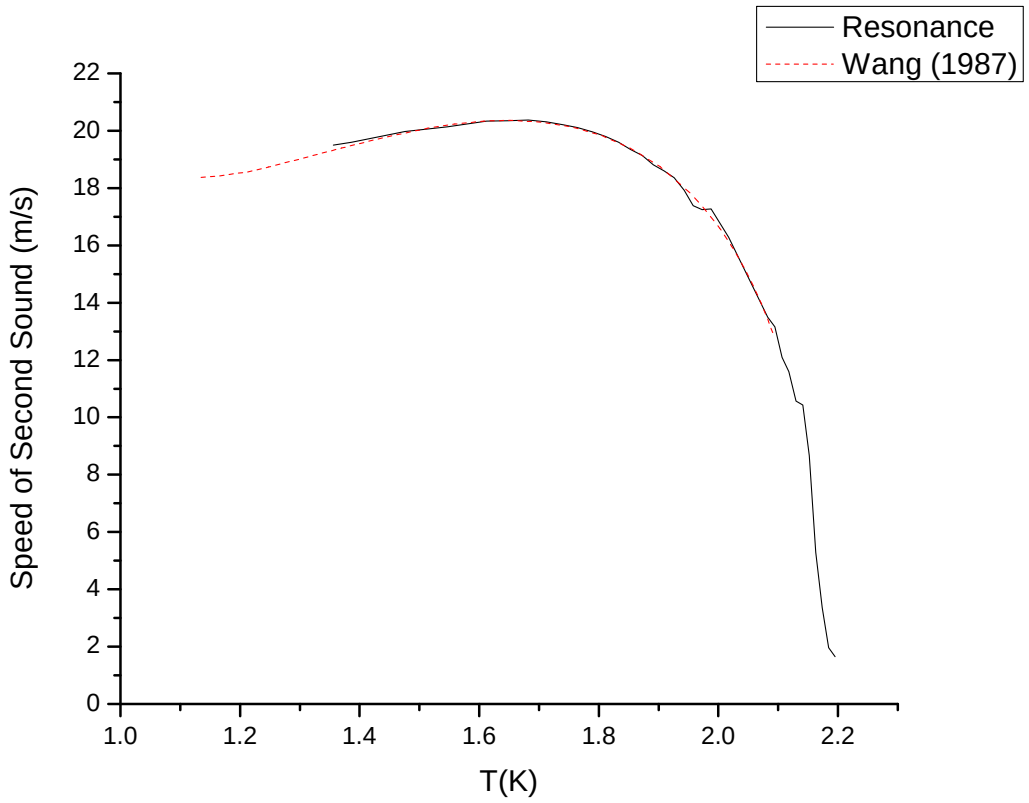

FIG. 10: Temperature dependence of the speed of second sound in the resonant geometry(in black). Also, data obtained by Wang (1985) for comparison. There is a high degree of correlation between the two data sets.

B. Error Analysis

The error for the resonance method as given by the MATLAB routine is given in Table 1.

Our apparatus for determining the pressure of the system gave an accuracy of $\delta \simeq \pm 0.5$ torr. We can estimate the resultant error in the second-sound velocity at any one temperature by treating the error as a perturbation to the vapor pressure-temperature relation $u(P(T)) = u(P_0(T) \pm \delta)$. Expanding yields $\frac{\Delta u}{u} = \frac{\delta}{u}\frac{du}{dP}$. In the critical region between 1.7 and 20 torr, the mean slope is $\simeq 0.1$ (m/s)/torr, and hence we find the error over this region to be $\frac{\Delta u}{u} \simeq 0.0025$, or 0.25%.

There is also an error due to the accuracy of the length of the resonating chamber. This error is given by $L_{(4K)} = 1.6246 \pm 0.0002$ inches. The corresponding error in velocity is $\frac{\Delta u}{u} = 0.0001$, or 0.0123%.

TABLE I: Error Contributions to Resonance Data

Source of Error	%
Pressure Uncertainty	0.25
Length of Resonating Chamber	0.0123
Data Fit	0.967

C. Results

The results from the resonant configuration can be seen in Figure 10. Our results show a high degree of correlation with previously obtained result (Wang et. all.).

In Figure 11, the results from the TOF method are compared with the resonance method. The TOF data fits the overall spline, but there is much greater more variation in the data.

V. CONCLUSION

The frequency sweep method produced more consistent results for the speed of second sound than the time of flight method, which was far more volatile. This variability was most likely a result of the poor signal-to-noise ratio, which tended to distort the initial rise of the voltage across the listening transducer. We could improve

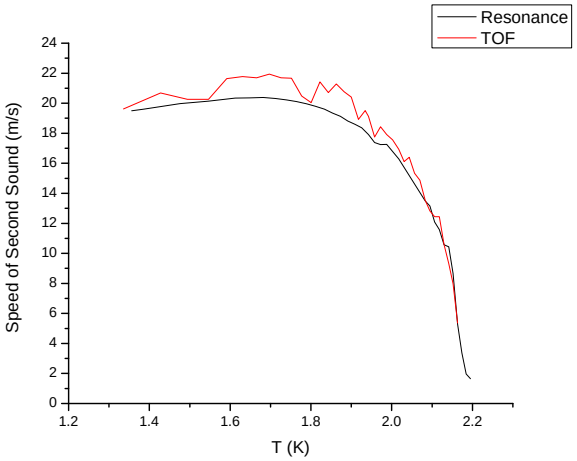

FIG. 11: Comparison between TOF (red) and resonant (black) configurations.

the reliability of this measurement with several changes to the experimental design. To increase signal-to-noise ratio, we can increase the DC bias on the listening transducer, and we can further amplify the drive pulse. These changes should lead to a stronger signal on pulse arrival; also, additional rings may be visible in the oscilloscope trace. Increasing the signal-to-noise ratio and incorporating more data points into the analysis should greatly improve the quality of the measurement.

Our frequency sweep method could be improved by incorporating a sensitive thermometer close to the resonant chamber, and with more precise temperature control. With better temperature regulation, the frequency step size could be decreased and the measurement time increased, which would allow for better frequency resolution.

Finally, though the noise method showed good promise in detecting resonance in air at room temperature, we did not detect any resonance in superfluid ^{4}He. This approach may have failed because our signal was not powerful enough to excite the resonant modes, or alternately because driving the He with noise raised the temperature in the bath.

Acknowledgments

We'd like to thank Professor Douglas Osheroff for his wisdom, guidance and oscilloscope, Chris Moon for his tireless help and support, Rick Pam for preventing experimental disasters, and Andrei Garcia for the gold-evaporation onto our Nucleopore filters.